Journal of the Mechanical Behavior of Biomedical Materials 167 (2025) 106979

Contents lists available at ScienceDirect

Journal of the Mechanical Behavior of Biomedical Materials

journal homepage: www.elsevier.com/locate/jmbbm

Cytocompatibility, fibroblast adhesion and proliferation on surface modified 3D-printed PEEK scaffolds

Pedro Rendas [a,*,1], Joana Amorim [b,c,1], Pedro Viana Baptista [b,c,**], Catarina Vidal [a,d], Lígia Figueiredo [e], Alexandra R. Fernandes [b,c], Bruno Soares [a,d]

[a] UNIDEMI, Department of Mechanical and Industrial Engineering, NOVA School of Science and Technology, NOVA University of Lisbon, 2829-516, Caparica, Portugal
[b] UCIBIO - Applied Molecular Biosciences Unit, Department of Life Sciences, NOVA School of Science and Technology, NOVA University of Lisbon, 2829-516, Caparica, Portugal
[c] i4HB, Associate Laboratory–Institute for Health and Bioeconomy, NOVA School of Science and Technology, NOVA University of Lisbon, 2829-516, Caparica, Portugal
[d] Laboratório Associado de Sistemas Inteligentes, 4800-058, Guimarães, Portugal
[e] IDMEC, Intertek Portugal, 4455-586, Porto, Portugal

ARTICLE INFO

Keywords:
Polyetheretherketone (PEEK)
Additive manufacturing (AM)
Surface modification
Scaffold
Fibroblasts

ABSTRACT

Polyetheretherketone (PEEK) is a high-performance thermoplastic that, when combined with Additive Manufacturing (AM), presents considerable advantages to produce customizable implantable medical devices. Despite this potential, PEEK's use as an implant material still presents challenges imposed by its bioinert nature. This study investigates the biofunctionalization of 3D-printed PEEK implants to enhance fibroblasts' cellular response due to their important role in the healing of connective tissue post-implantation. Different combinations of biofunctional features were investigated by surface modifying solid, porous, and surface-rough 3D-printed PEEK samples with the sulfonation treatment and incorporation of hydroxyapatite (HA) particles. The porous scaffold construct was designed based on a gyroid surface and then analysed using micro-CT and compression tests. Fibroblast culture assays were conducted to assess the effects of different surface morphologies on cellular adhesion and proliferation. Preliminary data of fibroblast metabolic activity on differently modified PEEK samples was also collected. Results from the experiments suggest that solid PEEK samples with rough surfaces and subjected to both sulfonation and HA incorporation procedures exhibit the most favourable environment for maintaining fibroblasts morphology and viability. Conversely, the lower adhesion and proliferation on smooth as-printed surfaces highlight the necessity for surface functionalization of 3D-printed PEEK. Additionally, results for metabolic activity paired with cell morphologies observed under SEM indicate that large-scale porous scaffolds may present less favourable environment for fibroblasts viability compared to solid surfaces. These findings offer valuable insights to 3D-printed PEEK biofunctionalization towards the improvement of fibroblast response, particularly considering their active role on extracellular matrix formation which is critical for connective tissue support and cohesion during the healing process after surgical implantation.

1. Introduction

Polyetheretherketone (PEEK) is a high-temperature thermoplastic material that has been considered for implant manufacture due to its biocompatibility. Its unique set of properties includes a high strength-to-weight ratio, chemical stability and resistance to radiation and in vivo degradation (Kurtz and Devine, 2007). Compared to metallic materials, PEEK's rigidity and strength are closer to that of human bone, while its compatibility with medical imaging techniques such as MRI and CT allow for better monitoring of the healing process (Green and Schlegel, 2001). Additionally, its lower rigidity helps avoid stress shielding of the treated bone, often associated with bone resorption and poor implant performance (Weinans et al., 1992). For these reasons, PEEK has been suggested as the leading candidate material for the replacement of

* Corresponding author.
** Corresponding author. UCIBIO - Applied Molecular Biosciences Unit, Department of Life Sciences, NOVA School of Science and Technology, NOVA University of Lisbon, 2829-516, Caparica, Portugal.
E-mail addresses: p.rendas@campus.fct.unl.pt (P. Rendas), pmvb@fct.unl.pt (P.V. Baptista).
[1] These authors contributed equally to this work as co-first authors.

https://doi.org/10.1016/j.jmbbm.2025.106979
Received 20 January 2025; Received in revised form 25 February 2025; Accepted 10 March 2025
Available online 10 March 2025

metals in the manufacture of load-bearing implants for trauma, orthopaedic, spinal and even dental treatment applications (Kurtz and Devine, 2007; Green and Schlegel, 2001; Kurtz, 2012; Zhang et al., 2025).

As a thermoplastic material, PEEK can be processed using Additive Manufacturing (AM) techniques, also known as three-dimensional (3D) printing, which can produce complex geometries with less material waste compared to conventional subtractive manufacturing techniques like machining (Sachs et al., 1993). With 3D-printing, components are created based on Computer-aided Design (CAD) virtual models, making these techniques flexible to design adjustments and more cost-effective in product development compared to other manufacturing techniques like injection moulding (Gibson et al., 2021). These advantages extend to medical applications where 3D-printed PEEK holds significant potential for the manufacture of patient-specific implants (PSIs) designed based on 3D data obtained from medical imaging (Kumar et al., 2021). Moreover, with the increasing accessibility to 3D-printing equipment, implant production can be moved to Point-of-Care (POC) facilities, providing a promising avenue for more personalized and effective medical solutions (Thieringer et al., 2022).

Printed PEEK's potential for the manufacture of PSIs is noteworthy, but its use in clinical practice is limited by challenges related to its mechanical performance and bioinert nature (Rendas et al., 2022). While PEEK's biocompatibility is well established (Wenz et al., 1990; Morrison et al., 1995; Rivard et al., 2002), its bioinertness has been addressed using different techniques that can enable implant-host interactions and improve bioperformance of PEEK as an implant material. These strategies for PEEK biofunctionalization can be divided as bulk or surface modifications of PEEK samples, like PEEK-matrix composites incorporated with bioactive compounds and surface-modified PEEK via surface coatings or physical and chemical treatments (e.g. acid etching) (Ma and Tang, 2014; Dondani et al., 2023). Within surface modifications, textured surfaces created with physical treatments can enhance the adhesion of primary cell lines like mesenchymal stem cells and fibroblasts (Briem et al., 2005; Ouyang et al., 2019; Ajami et al., 2017). Similarly, surface roughness created by sandblasting increased fibroblast cell adhesion (Porrelli et al., 2021) and osseointegration measured through pull-out tests on implanted samples (Sunarso et al., 2018). Alternatively, surface coatings with bone-like ceramic compounds, such as hydroxyapatite (HA) increased osteogenic differentiation (Lee et al., 2017) and promoted new bone formation on implanted samples (Johansson et al., 2018). Lastly, chemical treatments can modify PEEK's bioinert surface to improve cellular responses. Using organosilane compound, carboxyl groups were introduced into the surface of PEEK substrates, which improved the adhesion and proliferation of osteoblast (Zheng et al., 2015). Alternatively, the etching action of acid creates a microporous network on PEEK's surface that resulted in higher adhesion and proliferation of bone mesenchymal stem cells and pre-osteoblasts compared to untreated PEEK samples (Su et al., 2020; Li et al., 2020; Huo et al., 2021; Zhao et al., 2013). In addition to this, PEEK's surface modification can also aim for distinct biofunctionalities like enhanced immunological response achieved with bisphosphonation (Zhang et al., 2023) or antibacterial activity using silver coatings (Gao et al., 2017).

Apart from surface modifications, PEEK can also be architectured into complex porous constructs that may enable distinct biofunctionalities. In this regard, AM is uniquely capable of creating three-dimensional scaffolds with interconnected pores that allow vascularization, improving nutrient and oxygen supply (Abbasi et al., 2020), and favouring direct osteogenesis (Karageorgiou and Kaplan, 2005). Concerning PEEK, pore sizes from 100 to 700 μm have been suggested where larger pores showed better bone ingrowth and integration (Lewandrowski et al., 2000). Despite these outcomes, larger pore sizes also resulted in higher volume porosity which inevitably compromised the strength and rigidity of the scaffold. To avoid this, scaffold designs should look to obtain desired pore configurations without increasing volume porosity.

In addition to this, scaffold constructs can also be integrated with the abovementioned surface modification techniques to combine multi-scale features which can further enhance the bioperformance of PEEK scaffolds. Using a similar approach, bioglass scaffolds with macropores between of 300–500 μm combined with nanopores of about 20 nm enhanced adhesion of mesenchymal stem cells and were suggested to be more conductive to bone regeneration (Xia et al., 2022). This suggests PEEK's biofunctionalization may involve combining different multi-scale features, where macropores facilitate vascularization and bone ingrowth whereas rough surfaces with smaller-scale porosities support cellular adhesion and proliferation.

Nevertheless, most works on PEEK's biofunctionalization study osteogenesis-related responses with osteoblasts, considering their role in bone formation (Elhattab et al., 2020; Spece et al., 2020; Wong et al., 2021). However, the modification of PEEK can also achieve biofunctionalization based on the behaviour of other types of cells, where the interconnected pores of scaffold structures allow the migration of endothelial and fibroblast cells enabling vascularization and fibrogenesis within the pores (Mikos et al., 2002; Takaoka et al., 2024). These types of cells play an important role in the healing process after surgical intervention and thus, their responses determine implant performance. In a study where 114 custom-made 3D-printed PEEK implants were used in chest wall reconstructive surgery, lack of adhesion of surrounding tissue to the implant was identified as the sole post-operatory complication in 5 % of the population 1 year after surgery (Wang et al., 2022). Similarly, in another study where 45 patients underwent cranio-maxillo-facial reconstruction using PEEK PSIs, all reported post-operative complications were related to soft tissue adaptation (Gugliotta et al., 2024). In these cases, bone integration was not the issue, underlining the importance of also considering the integration with soft and connective tissues, even when considering bone-replacing implant applications.

Although the cellular interactions of differently functionalized PEEK samples with specific methods have been previously examined, there is a limited body of research that assesses the cellular responses to different biofunctional features within the same experimental setting. Some works have modified PEEK's surface by combining acid etching with HA, increasing cell viability and new bone formation (Sharifi et al., 2018; Yabutsuka et al., 2017, 2018; Masamoto et al., 2019). Despite their valuable contributions, the solid PEEK samples used in these works do not consider other features like surface roughness or the porous structures that can be obtained with 3D-printing. In a very interesting work, titanium dioxide polydopamine-coated PEEK that was 3D-printed into a scaffold and sputtered with HA not only resulted in increased mechanical properties but also achieved significant improvements in *in vivo* osseointegration, effectively applying biofunctional surface features to 3D-printed scaffolds (Jang et al., 2022). Nevertheless, the mentioned works still focus on osteogenesis-related responses and do not consider soft tissue integration as a critical aspect for the performance of PEEK implants. Considering this, this work aims to investigate and compare the effects of different combinations of 3D-printed PEEK biofunctional features in fibroblasts' response and identify the adequate surface features that constitute the most adequate environment for connective tissue adhesion and healing.

In this work, different combinations of biofunctional features were investigated, where solid, porous, and surface-rough 3D-printed PEEK samples were surface-modified with a sulfonation treatment and HA particle incorporation. The porous scaffold was designed according to the abovementioned requirements for pore size, interconnectivity, and structural integrity and was tested together with other printed specimens in both fully porous and solid-porous configurations. Fibroblast cell culture assays were conducted to assess the effects of the different combinations of surface morphologies on cellular adhesion and proliferation. Furthermore, preliminary data was collected on the metabolic activity of fibroblasts in culture on differently modified PEEK samples. Herein, we provide valuable insights into the biofunctionalization of 3D-

printed PEEK, particularly regarding fibroblasts behaviour and connective tissue's key role in implant performance, thus contributing to developments in surgical treatment applications of 3D-printed PEEK implantable devices.

2. Materials and methods

2.1. Materials and equipment

All samples used in the experiments were 3D-printed with neat PEEK filament (Apium PEEK 450 Natural, Apium Additive Technologies GmbH, Karlsruhe, Germany) with a diameter of 1.75 mm, density of 1.3 g/cm^3, tensile strength of 98 MPa and elastic modulus of 4 GPa (Table 1) (Apium PEEK 450 Natural Datasheet). The PEEK samples were printed on an Apium's P220 printer (Apium Additive Technologies GmbH, Karlsruhe, Germany) equipped with a 0.4 mm nozzle. This printer is designed for high-performance printing of high-temperature materials such as PEEK where a heating plate around the extruder regulates the temperature of the deposition region. Before printing, the PEEK filament was dried in the Apium F300 filament dryer (Apium Additive Technologies GmbH, Karlsruhe, Germany) for 4 h at 120 °C and then maintained at 60 °C for conditioning and printing.

2.2. Sample design and 3D-printing

Disc samples with 13 mm of diameter and 3 mm of height were printed for the experiments. Unmodified printed samples are separated into two configurations, smooth surface samples labelled as 'S' and rough surface samples labelled as 'R'. To obtain the rough printed samples, the filament was submersed in distilled water for up to one week before printing to leverage the hygrometric properties of PEEK. With this novel procedure, the evaporation of water absorbed by the filament upon extrusion results in an irregular rough surface on printed PEEK samples. Both these configurations were printed as solid samples, with 100 % infill to produce fully dense prints and as porous scaffold samples designed with large-scale interconnected channels which are herein labelled with the suffix 'P'. For these scaffolds, the samples were designed using the gyroid Triply Periodic Minimal Surface (TPMS), in SolidWorks (v.2023, Dassault Systèmes) where unit cell size and surface thickness were adjusted for the desired pore size and porosity percentage. The desired values for these parameters were set according to previously mentioned research remarks on porous design requirements.

With the samples designed, the 3D models' stereolithography (STL) files were imported into the slicer software Simplify3D (v4.1.2) where the G-code printing files were generated. All samples were printed with the circular face flat on the build plate with a 2-layer raft and an 18-line brim to ensure adhesion to the build plate. Other printing parameters, outlined in Table 2, were selected according to previous research results for the highest strength and density cylindrical test specimens (Rendas et al., 2023). In line with the methodology of this research, the extrusion flow was adjusted using a Python script that modifies extrusion based on a printed line's length. These adjustments are essential to avoid over-extrusion issues which tend to happen in small gap-filling movements in both the gyroid scaffold samples and in the innermost laps of the concentric deposition on solid samples. Furthermore, the surface rough samples also required extrusion adjustment by a factor of 0.9 due to volume increases after water absorption.

Considering these preparations, the samples were printed and labelled according to four groups, smooth samples 'S', rough samples 'R', and their respective porous scaffold counterparts, 'SP' and 'RP' as detailed in Table 3. Through these configurations, the effects of surface roughness and large-scale interconnected porous features on cellular interactions can be assessed and compared to solid PEEK samples.

Table 1
Apium PEEK 450 Natural Filament properties (Apium PEEK 450 Natural Datasheet).

Filament Material Properties	
Density, ρ [g/cm^3]	1.3
Elastic modulus, E [GPa]	4.0
Tensile strength, σ_m [MPa]	98
Tensile elongation, ε_m [%]	45
Glass transition temperature, T_g [°C]	143
Melting temperature, T_m [°C]	343

Table 2
Printing parameters set in Simplify3D.

FFF Printing Parameters				
Nozzle temperature	485 °C	Layer height		0.20 mm
Bed temperature	130 °C	Extrusion width		0.48 mm
Zone heater temperature	130 °C	Printing speed		600 mm/min
Deposition pattern	Concentric	Retraction	Distance	4 mm
Deposition sequence	Outside-In		Restart	0.2 mm
Raft layers	2		Z-lift	0.15 mm
Brim outlines	18	X/Y movement speed		4800 mm/min

2.3. Surface modification

Each of the four groups of 3D-printed samples was reproduced and subsequently submitted to sulfuric acid surface etching, commonly referred to as sulfonation treatment. This treatment was performed by immersing and stirring PEEK discs in sulfuric acid (95–97 % a.r., Chem-Lab NV, Zedelgem, Belgium) for a duration of 3 min. This sulfonation time was selected based on SEM observation of the surfaces of trial samples obtained with immersed during times ranging from 30 s to 5 min. Following the procedures documented in prior research, the sulfonated PEEK samples were subsequently rinsed in purified water and acetone (Zhao et al., 2013) followed by hydrothermal treatment at 100 °C for 4 h (Li et al., 2020; Ma et al., 2020). With this treatment, a nanostructured porous network is created in the surface of PEEK samples resulting in four additional groups identified with the prefix 'A' as shown in Table 3.

Additionally, the sulfonation treatment was replicated and complemented with a procedure for the incorporation of hydroxyapatite (HA) particles via chemical deposition following the same procedure detailed in previous studies (Sharifi et al., 2018; Almasi et al., 2014). For this, sulfonated samples were immersed in a 10 %wt/v suspension of HA (≥95 %, 1–100 μm, Bioceramed- Cerâmicos para Aplicações Médicas, Loures, Portugal) in purified water and continuously stirred for 5 h, after which water rinsing removed any excess particles. Particle incorporation was performed in each of the groups of sulfonated samples resulting in another four groups identified with the prefix 'HA'. All surface-modified samples were subsequently dried in an oven at 120 °C for 4 h. The sample labels for each disc preparation procedure are outlined in Table 3.

2.4. Sample characterization

Considering the neat surface PEEK discs, test specimens of configurations 'S', 'R', and 'SP' were 3D-printed to compare the compressive

Table 3
Labelling of samples according to different preparation procedures.

	3D-Printed		
	—	Acid-treated	
			HA-incorporated
Smooth	S	A-S	HA-S
	SP	A-SP	HA-SP
Rough	R	A-R	HA-R
	RP	A-RP	HA-RP

behaviour of the scaffold design and the rough printed samples with the behaviour of solid smooth printed PEEK. Additionally, a surface porous sample labelled as 'M-SP' was printed where the porous scaffold design used in samples 'SP' was limited to a 3 mm thickness of the top and bottom surfaces of the specimen, with the rest of the sample printed solid.

For each of these configurations, cylindrical compression test specimens with 13 mm diameter and 26 mm of height were 3D-printed and tested according to ASTM D695 guidelines. Compression testing between plates was performed for all samples at the standard test speed of 1.3 mm/min, conducted using a universal testing machine (INSTRON 1342, Instron Corp, Massachusetts, USA) equipped with a 250 kN load cell from which the modulus of elasticity and the offset yield strength at 0.2 % strain were calculated, all according to ASTM D695-96. For specimens 'M-SP', a second linear region was observed when plastic deformation occurs solely in the porous sections of the specimen. From this region, a second modulus was calculated, and the corresponding yield strength obtained at the proportional limit where R^2 from the linear regression fell below 0.998. All compression tests were repeated 5 times for each of the specimens' configurations.

Additionally, a compression test specimen of the scaffold configuration 'SP' was submitted for porosity analysis using micro-Computed Tomography (Micro-CT). This analysis was conducted at Micronsense-Metrologia Industrial (Leiria, Portugal) using a Phoenix V| TOME|X m 240 where the PEEK samples were scanned at 75 kV and 180 μA, with an angular increment for the scanning of 0.15° and spatial resolution 41 μm. The image data was analysed using a 3D tomographic reconstruction and analysis software (Volume Graphics 3.5.2 software, Volume Graphics).

2.5. Surface characterization

The different surface features of the disc samples were examined using a Scanning Electron Microscope (SEM) (model SU3800, Hitachi Ltd., Tokyo, Japan) with the detection of secondary electrons (SE) mode under high vacuum and with an accelerating voltage between 20 kV and 30 kV. For this, the non-conductive samples were gold-sputtered for about 90 s at a pressure of 0.1 torr, current between 10 and 20 mA, and voltage of about 1 kV under an argon environment.

The surfaces of solid disc samples were also characterized using surface roughness and wettability measurements. Surface roughness was measured using a portable profilometer (MarSurf PS 10, Mahr GmbH, Goettingen, Germany) programmed for a traversing length of 4.8 mm, velocity of 1 mm/s and equipped with a stylus of 2 μm. For each of the samples, a minimum of 3 roughness measurements were taken in the radial direction of the top surface of the discs and the report data was calculated according to ISO 16610-21. Water contact angle measurements were obtained with a goniometer (KSV CAM100, KSV instruments, Finland) which were also repeated 3 times for each sample.

2.6. Cell culture

Primary Dermal neonatal human Fibroblasts (PCS-201-010) were obtained from American Type Culture Collection (ATCC®, United States). Cell culturing and maintenance were done in Dulbeco's Modified Eagle Medium (DMEM, Gibco™ by Life Technologies, United States), supplemented with 10 % (v/v) Foetal Bovine Serum (FBS; Gibco™ by Life Technologies, United States) and 1 % (v/v) Penicillin and Streptomycin. For culture maintenance, the medium was further supplemented with 5 ng/mL of Fibroblast Growth Factor (FGF, Sigma-Aldrich, United States). Incubation of the cells was performed at 37 °C, with 99 % humidity and 5 % (v/v) CO_2 (Lenis-Rojas et al., 2017).

2.7. Sample preparation for cell experiments

Before use in cell experiments, the samples were washed and sterilized. Briefly, the samples were incubated in 70 % Ethanol for 1 h in a shaking incubator. Following the drying of the samples, these were again incubated in Phosphate Buffered Saline (PBS) for another hour in a shaking incubator. Afterwards, the samples were dried and autoclaved. Then, the samples were incubated in sterile PBS overnight to balance the surface charges. Finally, the samples were incubated in DMEM, for 4 h immediately before the beginning of the cell experiments, to enrich the samples in nutrients and facilitate the cell adhesion process.

2.8. Cell adhesion

Samples were inserted individually in wells of 24-well plates. The fibroblast suspension was prepared in DMEM supplemented as previously described, except without the addition of FGF, at a concentration that guaranteed the presence of 1.08×10^5 cells per 700 μL of cell suspension. The seeding value was calculated based on the growth area relation and 20 % extra was added to account for the extra surface area of the samples. Then 700 μL of the cell suspension was added over the samples or into empty wells, for experiment control. Cells were left to proliferate in an incubator at incubated at 37 °C, with 99 % humidity and 5 % (v/v) CO_2, for four days.

2.9. Cell counting

The capability of cells to adhere and proliferate in the samples was assessed through trypsinization of cells in the samples and corresponding wells occurred separately. The process consisted of the removal of the growth medium following washing with PBS. After the removal of PBS, a 10-min incubation with the dissociation agent TrypLE™ Express (Gibco™ by Life Technologies, United States). Following the inactivation of the dissociation agent with DMEM, the mixtures were centrifuged individually. Cell counting was performed via the Trypan Blue exclusion method with the use of the CytoSMART Exact automated cell counter (Axion BioSystems, Atlanta, United States).

2.10. Cell viability

The cells were cultured as previously detailed for the assessment of fibroblasts viability in the two environments (well bottom and samples). Firstly, the cells were removed from the wells and put into new 96-well plates, and 80 μL of fresh medium and 20 μL of the CellTiter 96® Aqueous One Solution Cell Proliferation Assay kit reagent (Promega, Madison, United States) were added to the wells. Following a 1-h incubation period, the total volume of medium was placed into wells of a 96 well plate, and the absorbance at 490 nm was read using a microplate reader, Tecan Infinite M200 (Tecan, Mannedorf, Switzerland). With this method, cell viability can be indirectly assessed as a measure of mitochondria viability, as only metabolically active cells will reduce 3-(4,5-dimethylthiazol-2-yl)-5-(3-carboxymethoxyphenyl)-2-(4-sulfophenyl)-2H-tetrazolium, inner salt (MTS) to formazan, due to their active mitochondrial dehydrogenases (Lenis-Rojas et al., 2017; Choroba et al., 2019).The background absorbance value was obtained from a well containing only the mixture of medium and reagent (control well), and this value was then subtracted from all other absorbances.

2.11. Cell assay data treatment

All values represent the ratio between the values/counts for the isolated sample by the corresponding control well value. This is represented below (1), wherein X can be replaced with either the number of cells or fluorescence values to obtain the values represented for these assays. The ratios obtained represent the similarity between the sample and the corresponding well which represents the ideal growth environment.

$$Ratio = \frac{X_{Cells\ on\ sample}}{X_{Cells\ on\ well}} \quad (1)$$

2.12. Scanning electron microscopy (SEM) for fibroblasts morphology

Following the four-day incubation period, samples containing and not containing Fibroblasts were washed with PBS and incubated with paraformaldehyde (PFA) for 30 min. After fixation of the samples, these were washed three times and stored with PBS at 4 °C.

Before Scanning Electron Microscopy (SEM) observation, these samples were dried and fixed to the SEM stub using aluminium tape. After this the stub with the samples was gold sputtered following the same procedure described in subsection 2.5. to obtain SEM images of the cells fixed on the non-conductive PEEK samples. To distinguish cellular bodies from other features that could be created by cell culture procedures, SEM images of cell-cultured samples were compared with images of samples that underwent the same procedure but were incubated without the presence of cells.

2.13. Statistical analysis

Statistical analysis was performed using the GraphPad Prism program (version 8.0.1). The non-parametric two-way ANOVA test with multiple comparisons where the Tukey method was used to compare different PEEK constructs for both fibroblast growth and distribution, by estimating the p-value. Results were considered statistically significant for $p < 0.05$.

3. Results and discussion

3.1. Sample design and compressive behaviour

Considering the role of additive manufacturing in the production of implantable medical devices, the ability to produce intricate designs with 3D-printing is often leveraged for the fabrication of porous scaffolds where different designs can have different outcomes in both the mechanical behaviour and the bioperformance of the samples. In this work, the design for scaffold samples SP and surface-modified versions thereof were obtained based on pore configuration requirements for implantable medical devices. One of the main requirements for scaffold design is the presence of sufficiently large pores that allow cell proliferation and vascularization, which should be arranged in an interconnected network to enable oxygen and nutrient transport deep into the scaffold (Jarman-Smith et al., 2012). Pore size and interconnectivity are typically fulfilled at the expense of the design's volume porosity where a highly interconnected network of larger pores will result in a scaffold design with considerably lower strength and rigidity compared to solid designs (Karageorgiou and Kaplan, 2005). This makes the structural integrity another key requirement for scaffold design, especially considering the load-bearing implant applications where 3D-printed PEEK displays its potential.

The gyroid TPMS was selected for the design which, like the Schwarz diamond and primitive, displays an interconnected pore configuration that can be 3D-printed while retaining effective load transfer through the lattice structure. With this, additively manufactured TPMS biomaterial scaffolds have the potential to assimilate the topological and mechanical properties of bone, making them highly suitable for bone tissue engineering applications (Restrepo et al., 2017; Bobbert et al., 2017; Valainis et al., 2019).

PEEK scaffolds have been previously 3D-printed based on these TPMS geometries where the designs presented a direct relation between pore size and scaffold porosity (Spece et al., 2020). In these printed PEEK structures, the compressive properties were found to decrease with the designed porosity percentage (Spece et al., 2022). However, porosity can be decreased for the same pore size by applying a scaling factor to the unit cell structure size and thickness. With TPMSs like the gyroid, the increase in strut thickness results in a higher volume fraction for the scaffold design and results in a stronger and more rigid structure (Nsiempba et al., 2021; Panesar et al., 2018). To avoid the reduction of pore size with the increase of volume fraction, cell size must be increased to allow the increase of the scaffold strength while retaining the desired pore size and interconnectivity.

Considering this, the scaffold design of samples SP used in this work was obtained by increasing the strut thickness, *T*, and unit cell size, *S* of the gyroid TPMS unit cell following the procedure illustrated in Fig. 1a. For this, initial iterations were performed to adjust designed pore size until the smaller dimension of the pore cross-section, labelled as dimension *P* in Fig. 1a measured approximately 600 μm. To obtain this dimension, the dimension *P* in the design model had to be adjusted to 800 μm while the designed pore volume fraction was kept at approximately 40 %. With this, a cylinder compression specimen was 3D-printed and submitted to porosity analysis using micro-CT to compare sample porosity, strut thickness, pore size, and other measurements to the designed dimensions (Table 4).

The results from micro-CT analysis attest to the printability of the gyroid design implemented for scaffold samples SP. The average measured pore size of 458.4 μm agrees with the pore size range between 100 and 600 μm suggested for cell proliferation and vascularization of macroporous scaffolds (Abbasi et al., 2020; Karageorgiou and Kaplan, 2005; Jarman-Smith et al., 2012) while the average strut thickness measured 834.8 μm. This resulted in a volume porosity percentage of just 24 % which is much lower than the porosity of previously researched printed PEEK scaffolds (Elhattab et al., 2020; Spece et al., 2020; Wong et al., 2021) and showcases the potential for a scaffold design with higher strength and rigidity. However, due to 3D-printing's deposition, both the measured porosity and pore size of the printed scaffold were lower than their respective designed dimensions, which can mean that the interconnectivity of the porous network was compromised. This was assessed by examining the tomography of the micro-CT data along longitudinal and transversal cross-sections of the sample, as shown in Fig. 1b. Through this analysis, the interconnectivity of the porous network was considered intact. Animated images demonstrating this analysis can be found in the (Supplementary Fig. 1).

Following this, cylindrical test specimens were tested to compare the compressive behaviour of scaffold samples SP and surface-rough samples R to the behaviour of solid printed samples S. In addition to this, surface macroporous samples M-SP were also tested to represent the case where porous features are solely implemented at the functional interface. These printed samples can be seen in Fig. 1c, together with their respective highest-strength stress-strain curves. Additionally, compressive property results were compared along with density estimates based on the samples' mass and dimensions Table 5.

Compared to solid samples S, both R and SP resulted in significantly lower rigidity and strength. With sample R, the rough surface is obtained when the water absorbed by the filament evaporates upon extrusion creating open porosities in the deposited material. Although these porosities can be desirable for cell interactions, these features can also be present in the interfaces between the layers when the samples are 3D-printed, thus hindering interfacial bonding and resulting in the presence of internal void defects. For these reasons, the estimated density for sample R was about 12 % lower than the density measured for sample S, despite both being obtained with the same printing file. With this, the procedure to create surface-rough printed PEEK leveraging on its hygrometric ability presented in this work also results in a significant reduction of both its rigidity and strength in relation to smooth-printed PEEK samples.

With scaffold samples SP, the lower strength and rigidity were expected considering that the designed porous network results in a smaller effective cross-section area for load support. Despite this, all tested scaffolds withstood the compressive loading through plastic deformation without fracture, attesting to the structural integrity and printability of the scaffold design presented in this work.

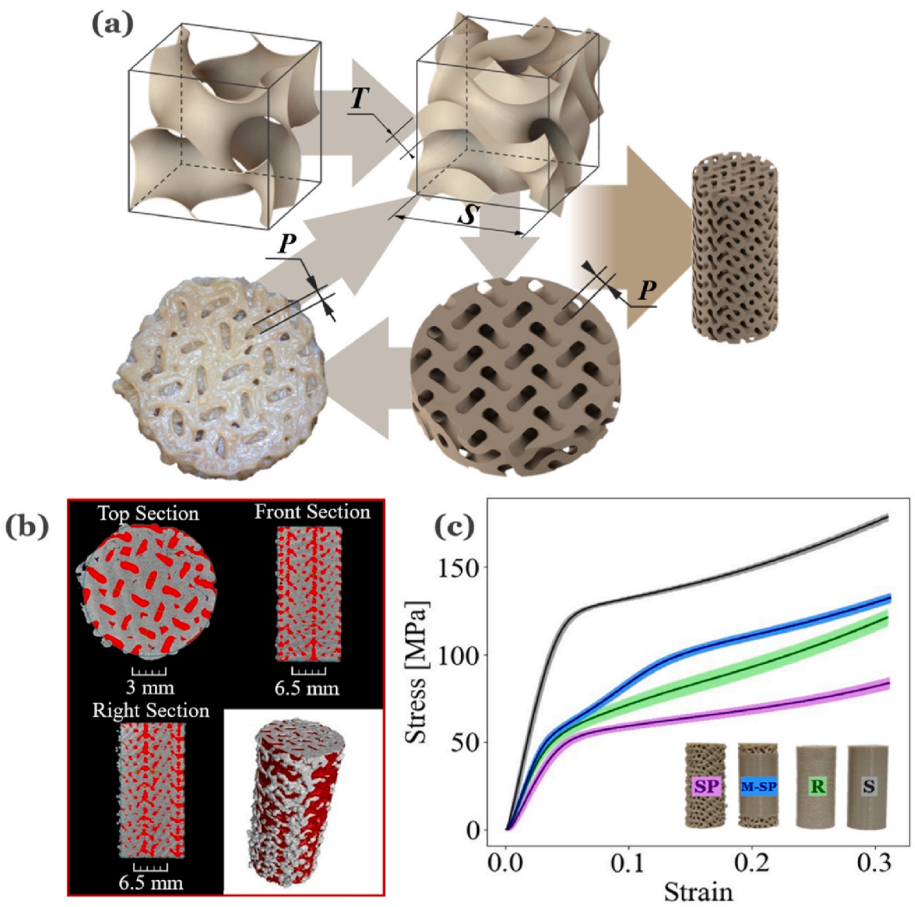

Fig. 1. Gyroid design iteration for scaffold CAD model dimensioning (a), porosity analysis of void volume (red) and its interconnectivity in Micro-CT data visualization software (b), and engineering stress-strain curves and standard deviations plot from compression testing of the highest strength as-printed samples (c). Animated images of Micro-CT interconnectivity assessment can be found in supplementary documentation Fig. 1. (For interpretation of the references to colour in this figure legend, the reader is referred to the Web version of this article.)

Table 4
Comparison between as-designed dimensions and micro-CT measurements from test specimen of sample SP.

	As Designed	Micro-CT
Height [mm]	26.00	25.81
Diameter [mm]	13.00	12.65
Void Volume [mm^3]	1376.90	740.61
Solid Volume [mm^3]	2074.14	2346.23
Surface Area [mm^2]	6372.15	7039.35
Dimension *P* [mm]	0.800	0.604 ± 0.044[a]
Strut Thickness [μm]	——	834.8 ± 178.0
Pore size [μm]	——	458.4 ± 147.6
Porosity [%]	39.9	24.0

[a] Measured through microscopic images (ISM-PM200sb, Insize Co., Suzhou, China).

In addition to this, there is the unique ability of 3D-printing to implement these designs solely at the functional interface of the component and therefore, reduce its consequences on the mechanical behaviour of printed PEEK components. This was tested with surface porous samples M-SP which display a higher Young's modulus of 1.87 GPa and yield strength of 44.1 MPa compared to the full scaffold SP. Interestingly, as seen in Fig. 1c, the stress-strain curve of these samples is characterized by two linear regions where the second represents the compound effect of the elastic deformation of the solid region with the pore compression plastic deformation of the scaffold sections of the specimen. With this configuration, the proportional limit compressive strength obtained from the second linear region after pore compression averaged 91.4 MPa, closely resembling the strength of solid samples S. This suggests that, if pore compression is admitted, large-scale porosities can be 3D-printed at the functional interface resulting in a higher strength functionally graded design developed towards the implant's application requirements. Nevertheless, both the yield strength and rigidity of the printed scaffolds obtained in this work sit within the range of the compressive properties of trabecular bone (Su et al., 2023) and are significantly higher than previously presented for 3D-printed PEEK scaffolds (Spece et al., 2020).

3.2. Surface characterisation

The sample configurations used in this work result from combinations of the different printed samples with the surface modifications of acid etching and particle incorporation. The goal of testing these combinations is to assess both the individual and compound influence of different surface features in the behaviour of fibroblast cells, which are critical for evaluating the biocompatibility and effectiveness of implant materials. For this, surface characterisation of the samples was conducted according to these features, measuring surface roughness and wettability while surface morphologies were observed under SEM.

Surface roughness measurements were exclusively performed on solid disc samples (S, A-S, HA-S, R, A-R, HA-R) due to the profilometer's need for a continuous surface, which scaffold samples do not possess (Table 6). In these measurements, all rough printed samples (R, A-R, HA-R) presented higher surface roughness compared to the corresponding smooth printed samples (S, A-S, HA-S), with a strong statistical significance ($p < 0.01$) (Fig. 2a). These differences are evident when

Table 5
Compressive properties and density results of as-printed PEEK cylindrical specimens.

	Estimated Density, ρ [g/cm^3]	Young's Modulus, E_1 [GPa]	Compressive Yield Strength, $\sigma_{0.2\%}$ [MPa]	Strain at Yield, $\varepsilon_{0.2\%}\left[l/l_0 \times 100\%\right]$	Young's Modulus, E_2 [GPa]	Compressive Proportional Limit Strength, σ_{PL} [MPa]	Proportional Limit Strain, $\varepsilon_{PL}\left[l/l_0 \times 100\%\right]$
S	1.264 ± 0.021	3.12 ± 0.06	94.4 ± 1.7	3.54 ± 0.15	–	–	–
R	1.116 ± 0.094	1.67 ± 0.14	36.7 ± 2.2	2.84 ± 0.34	–	–	–
SP	0.939 ± 0.028	1.33 ± 0.08	38.3 ± 0.6	3.37 ± 0.32	–	–	–
M-SP	1.126 ± 0.007	1.87 ± 0.14	44.1 ± 0.7	2.93 ± 0.28	0.47 ± 0.01	91.4 ± 1.3	12.14 ± 0.44
Cortical Bone (Su et al., 2023)	1.92	6–30	–	–	–	–	–
Trabecular Bone (Su et al., 2023)	0.05–0.3	0.01–3	2–70	–	–	–	–
Mandible Trabecular Bone (Misch et al., 1999)	0.85–1.53	0.004–0.126	0.22–10.44				

Table 6
Surface roughness measurements of smooth and rough printed samples with differently modified surfaces.

	Smooth			Rough		
	S	A-S	HA-S	R	A-R	HA-R
Ra [μm]	6.452 ± 0.115	4.767 ± 0.283	5.389 ± 0.336	12.275 ± 1.142	8.012 ± 0.791	6.758 ± 0.139
Rz [μm]	29.924 ± 2.394	21.030 ± 0.450	25.802 ± 1.759	64.175 ± 8.853	40.088 ± 3.172	36.483 ± 0.565
Rmax [μm]	35.944 ± 1.410	27.994 ± 0.784	43.567 ± 9.569	102.289 ± 17.811	63.114 ± 17.790	56.683 ± 4.385
Rt [μm]	39.437 ± 2.805	29.969 ± 3.218	44.335 ± 9.544	106.743 ± 18.678	72.556 ± 23.352	61.735 ± 7.010

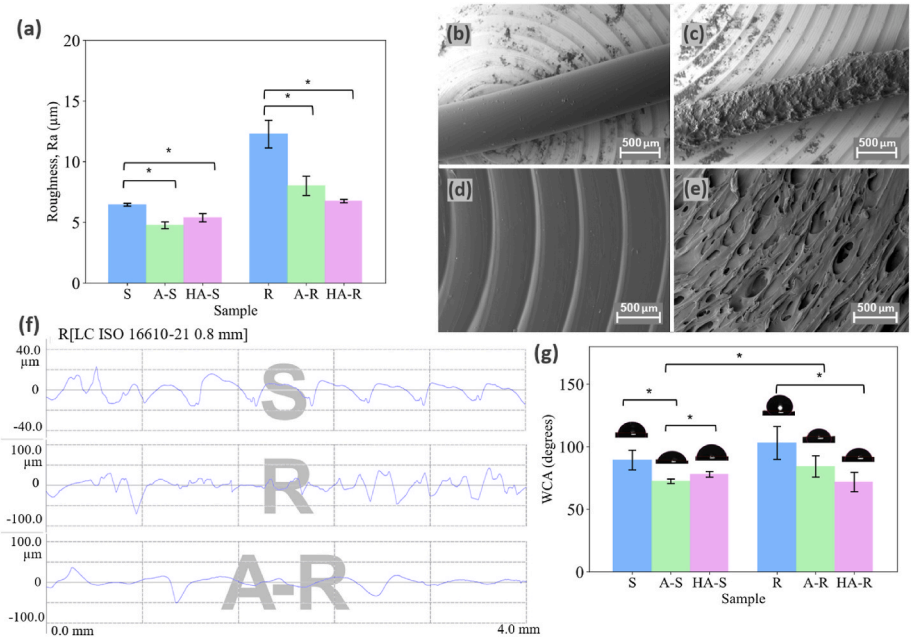

Fig. 2. Surface roughness R_a results for solid samples (a); SEM micrographs comparison between smooth (b) and rough (c) extruded filament and top surfaces of respective smooth (d) and rough (e) printed samples; surface profile comparison between solid samples S, R and A-R (f); Surface water contact angle plot for untreated, acid treated and particle incorporated solid samples. Statistically significant differences indicated by * ($p < 0.05$).

comparing SEM images of both these surface configurations (Fig. 2 b, c, d and e). Using this method to produce surface rough printed PEEK, the evaporation of the absorbed water forms protrusions in the extruded material (Fig. 2c) which when combined with the deposition movement results in a highly irregular surface (Fig. 2e). Comparatively, this surface is considerably more textured than the regularly printed filament (Fig. 2b) and deposition (Fig. 2d). This is also evident in the surface profiles of these samples shown in Fig. 2f where the "m" shaped profile characteristic of printing deposition seen with samples S cannot be identified in the profile of samples R.

These surface features observed in rough printed samples can be described as large-scale open porosities which are very different from the morphologies of rough PEEK surfaces through other methods like sandblasting (Porrelli et al., 2021). Compared to these methods, the rough PEEK surface presented in this work could similarly improve cell attachment through the increase of surface area or improve adhesion with surrounding tissue without the need for additional post-processing of as-printed samples. Despite this, as seen previously, creating these

rough surfaces corresponds to a reduction of the strength and rigidity of printed PEEK thus limiting the use of this method. Nevertheless, as proposed for the porous construct, these rough surfaces could be limited to functional interfaces where tissue adhesion is required.

Considering the surface modification of printed samples with sulfonation, the acid etching action reduced roughness by corroding surface irregularities which are more exposed to the acid in terms of surface area. This is particularly evident in sample R where sulfonation resulted in a much lower surface roughness for sample A-R and shows that, although it creates a small-scale porous network on PEEK's surface, sulfonation can also diminish larger-scale surface features. Apart from this, the influence of HA incorporation was found to be statistically insignificant in the surface roughness of both smooth and rough samples, even though there is the possibility of particles accumulating in rough surface irregularities and reducing the surface roughness with samples HA-R.

Regarding the wettability of the different samples, the water contact angle on smooth PEEK samples S averaged 89.4° while on rough samples R the average angle of 103.0° suggests a more hydrophobic surface (Fig. 2g). However, considering that both samples should have same material properties and corresponding surface energy, this difference in wettability could be caused by interference of the rough surface in the contact of the water droplet. For this reason, wettability measurements on rough surfaces show higher deviations, making the comparison to their smooth counterparts of low significance ($p > 0.05$). Despite this, wettability measurements on smooth samples show that the sulfonation treatment increases surface hydrophilicity between samples S and A-S ($p < 0.05$), which is then slightly lowered by HA incorporation from A-S to HA-S ($p < 0.05$). This increase in wettability with sulfonation agrees with previous works on acid-treated PEEK samples (Huo et al., 2021; Almasi et al., 2014; Wang et al., 2019; Huang et al., 2001) although other works also report on the decrease of PEEK's hydrophilicity with similar treatments (Li et al., 2020; Zhao et al., 2013; Ma et al., 2020).

The sulfonation of PEEK samples can produce different outcomes depending on PEEK's material properties, the type of acid used and treatment parameters like etching time, acid concentration, and post-etching treatment. In the mentioned works, the acid etching procedures vary considerably making it difficult to compare the etching degree of PEEK samples between different works. For this reason, the sulfonation time of 3 min used in this work was selected based on SEM images of trial-run sulfonated PEEK samples. With this treatment, the typical light-brown colour of PEEK samples turns to white even before HA incorporation (Fig. 3a), evidence of the sulfuric acid's modification of PEEK's surface. Under SEM observation, sulfonated samples show a nanoporous network (Fig. 3b) similar to the ones presented in previous works (Zhao et al., 2013) as well as its subsequent incorporation with hydroxyapatite particles (Fig. 3c). Nevertheless, SEM observation of the treated surfaces also revealed that the sulfonation degree varies along the samples' surface and that HA particles tend to agglomerate in surface irregularities created with the sulfonation treatment (Fig. 3d).

The sample configurations utilised in this study integrate different combinations of surface characteristics that play a role in the cellular interactions with 3D-printed PEEK. The morphologies obtained with the surface modification procedures closely align with those documented in previous research on PEEK biofunctionalization. Through these configurations, this study provides a framework for evaluating the optimal surface functionalization methodology for 3D-printed PEEK regarding the effects of different morphologies on the cytocompatibility, adhesion, and proliferation of fibroblast cells.

3.3. Cytocompatibility, adhesion and proliferation

Fibroblasts collected from PEEK samples were counted and normalized against the bottom of the corresponding cell culture-treated well. The polymer at the bottom of cell culture wells are treated to create an ideal environment for cell adhesion and proliferation. Thus, the comparison of the number of fibroblasts in each environment (PEEK samples and well bottom) was used as an indication of the preferred environment for fibroblast growth. Specifically, if the PEEK samples did not present a welcoming environment for fibroblast adhesion and growth, it would be expected that the number of cells in these samples would represent a negligible percentage of the total cells. The conduction of these studies after an adequate interval reduces the effects of random cell distribution at time of seeding. However, this was not the case since all PEEK constructs show an average distribution higher than 30 % of the total cells present (see Supplementary Fig. 2). This value is even more significant when accounting for the fact that the initial seeding accounted only for a 20 % increase in growth area. Thus, PEEK constructs, despite the different responses enabled by surface modification or porosity profile, appear to provide a minimally adequate environment for fibroblast

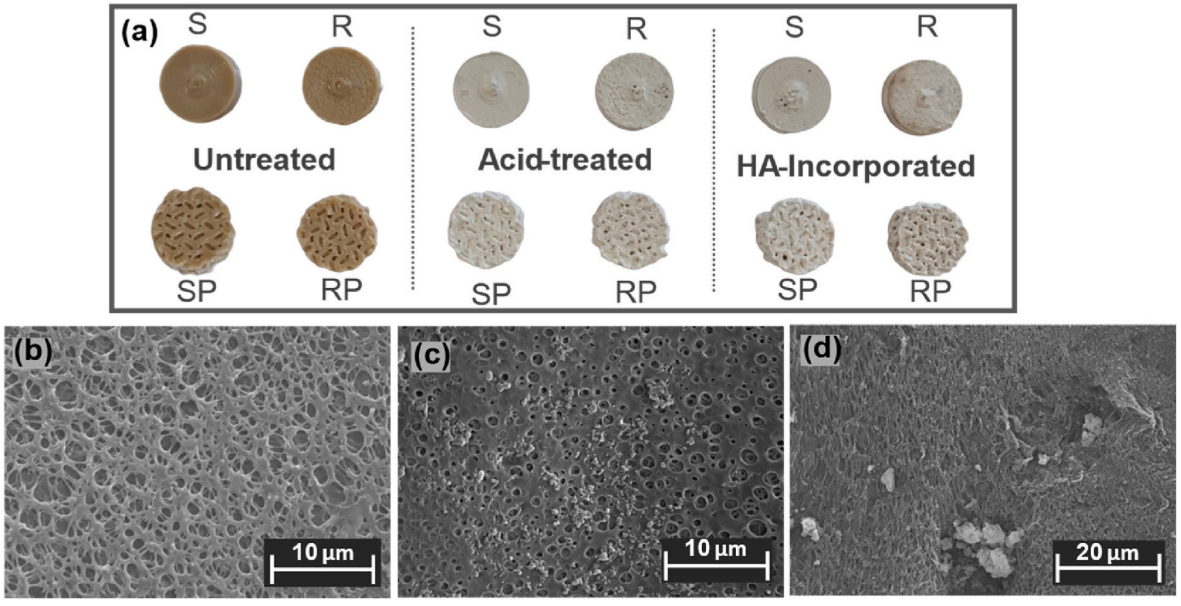

Fig. 3. Sample surface appearance and colour (a), and SEM micrographs of the surface morphology of solid printed samples after acid treatment (b) and after particle incorporation (c, d). (For interpretation of the references to colour in this figure legend, the reader is referred to the Web version of this article.)

adhesion and proliferation. This suggests that PEEK samples may be good candidates for connective tissue adhesion, which is essential for adequate recovery and proper function of the prosthesis.

Results for fibroblast growth, distribution, and metabolic activity are summarised in the heatmap of Fig. 4 and all data presented is representative of ratios calculated as in (1). Both values for cell growth and distribution are calculated based on the cell counting data, however these values represent different aspects as cell growth is calculated based on the total amount of seeded cells at the beginning of the experiment. Distribution only considers the data collected at the end of the experimentation period. Taking both analyses into account, it is possible to assess the preference of fibroblasts to adhere on sample surfaces separately from their distribution to growth environments.

Considering cell growth, sample configuration HA-R presents a ratio of 0.80 ± 0.03, making it the most like the profile presented by the bottom of the well. Given that the well bottom presents the most welcoming environment for culture and proliferation of fibroblasts, this ~80 % similarity between growth profiles suggests that the rough surface combined with sulfonation, and particle incorporation modification of samples HA-R, is adequate for fibroblast growth. Compared to other configurations, the differences in cell growth to HA-R were found to be statistically significant ($p < 0.05$) for all samples except for configurations A-SP, HA-SP, and HA-S. These samples presented fibroblast growth values of 0.61 ± 0,02, 0.57 ± 0.09, and 0.65 ± 0.07 respectively, representing an intermediate level of cell growth. Conversely, cell growth profile difference was most statistically significant ($p < 0.0001$) for as-printed smooth samples S (0.34 ± 0.11), highlighting the need for modification of 3D-printed PEEK's surface features to improve cellular interactions.

Cell distribution (well bottom vs. sample) results, similarly to cell growth data, show a statistically significant difference between HA-R and all samples with a ratio value of 0.79 ± 0.03 ($p < 0.05$). The exceptions were configurations A-SP, HA-SP, and HA-S. Likewise, these constructs that showed no statistically significant difference ($p > 0.05$) to HA-R had mean fibroblast distribution ratios of about 0.61 ± 0.03 for A-SP, 0.61 ± 0.05 for HA-SP, and 0.62 ± 0.04 for HA-S. These results reflect a more balanced distribution of fibroblasts between particle-incorporated samples and the well bottom, particularly for HA-R samples, further supporting the results observed for fibroblast growth. Moreover, these results for cell growth and distribution on sulfonated samples support the cytocompatibility of acid-etched surface modifications, consistent with the findings of previous studies (Zhao et al., 2013). Once again, the most statistically significant difference ($p < 0.0001$) was found when comparing the constructs HA-R with as-printed samples S that present a ratio value of 0.33 ± 0.11.

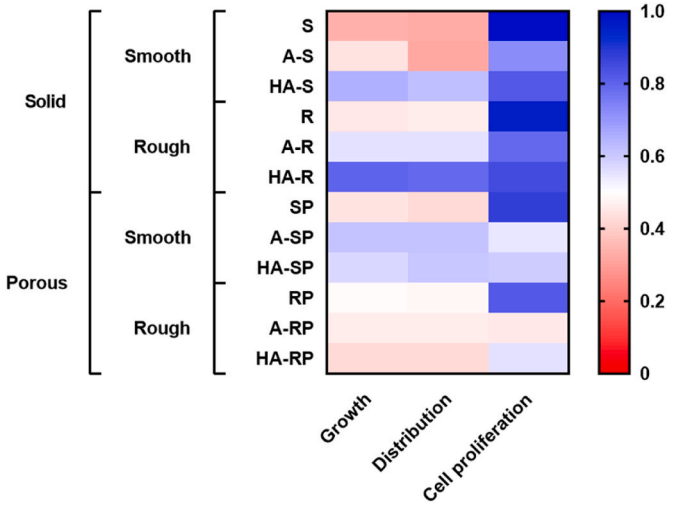

Fig. 4. Illustrative heat map of averaged ratios for cell growth, distribution and metabolic activity for different sample configurations. The ratios are between the values for the samples and the corresponding well. Values range from 0 (red) to 1 (blue) with 1 corresponding to an equality between the values for the sample and well and 0 corresponding to no similarity between the two. All values for fibroblast growth and distribution are representative of at least two independent experiments, each with at least three replicates. Metabolic activity data is only preliminary as it resulted from one single experiment. Further information can be found in supplementary documentation Fig. 2 and 3. (For interpretation of the references to colour in this figure legend, the reader is referred to the Web version of this article.)

No other comparison of values among the different constructs, either related to fibroblast growth or distribution showed statistically significant differences, which supports that HA-R presents the most favourable combination of surface modifications to create an adequate growth environment for these cells. Furthermore, the differences between the growth and distribution of fully modified rough samples HA-R and as-printed samples S show that cellular interactions with 3D-printed PEEK can be significantly improved by the surface modification procedures described in this work, particularly when the rough printed PEEK is combined with nanoscale porosity features incorporated with HA particles.

Although not statistically significant, both the distribution and growth values of fibroblasts seem to indicate that, with the solid PEEK constructs of samples S and R, there is a tendency for sulfonation to create a better growth surface with the implementation of HA particles further increasing such a tendency. This can be related to the increases in hydrophilicity seen with both steps of the surface modification procedure (Fig. 2g). When looking specifically at the rough-porous samples RP, an opposite tendency appears where surface treatments create a worse environment for cellular growth. Nevertheless, with smooth surface porous samples SP, both the sulfonation and the presence of HA particles seem to exhibit a similar tendency to smooth solid samples S. However, in this case, there does not seem to exist a combinatory effect at play between the sulfonation treatment and particle incorporation. Together, these results seem to indicate a tendency for smooth PEEK scaffolds SP to be more benefitted by sulfonation and HA particle presence than rough PEEK scaffolds RP where the surface roughness already constitutes a more adequate environment for fibroblast adhesion and proliferation.

Additionally, preliminary data on cell viability was obtained through the MTS assay (Supplementary Fig. 3). Results were normalized as previously done for the growth and distribution results. The obtained values were overall lower for porous samples than for smooth samples (Fig. 4). These results suggest that, despite the potential of scaffold structures for vascularization to allow nutrient and oxygen transport, cell migration within the porous network can also injure metabolic activity.

Cell adherence, morphology and distribution in the different samples were assessed through SEM observation and using as comparison sample surfaces that were incubated in the absence of cells. The observation of cells adhered and spread thinly on the samples' top surfaces was only possible under high contrast imaging for solid samples R and S (Fig. 5). Conversely, on porous samples, cellular bodies are more easily identified if these are spreading across porous features and around HA particles as Fig. 6 shows. With this, cell morphology was analysed and compared for the different sample configurations.

The observation of SEM images allowed for the comparison of cell morphologies between corresponding solid and porous constructs as shown in Fig. 7. When on solid samples, like HA-R (Fig. 7a and b), fibroblasts show a star-like morphology (Fig. 7c). Additionally, when we look at its porous equivalent, sample HA-RP, fibroblasts present a more elongated morphology with extracellular matrix extensions anchoring them to the surface and connecting them to other fibroblasts (Fig. 7d and e) which could be suggesting cellular stress with the cells "bridging the gaps" in the samples. Conversely, the star-like morphology (Fig. 7c) has been described in active myofibroblasts or wound fibroblasts expressing

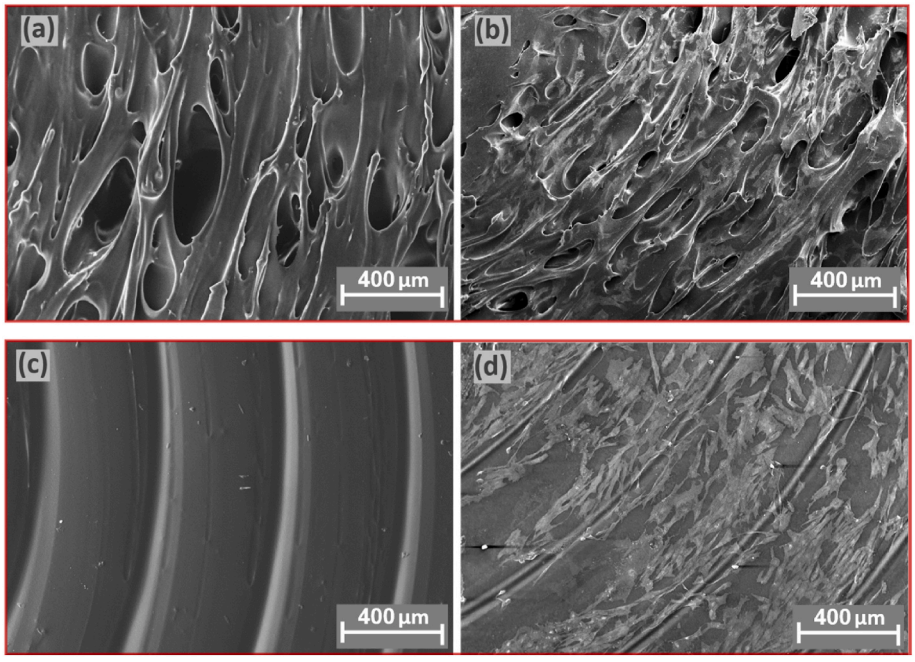

Fig. 5. High contrast SEM micrograph comparison between rough samples R (a, b) and smooth samples S (c, d) cultured without (left) and with cells (right), respectively.

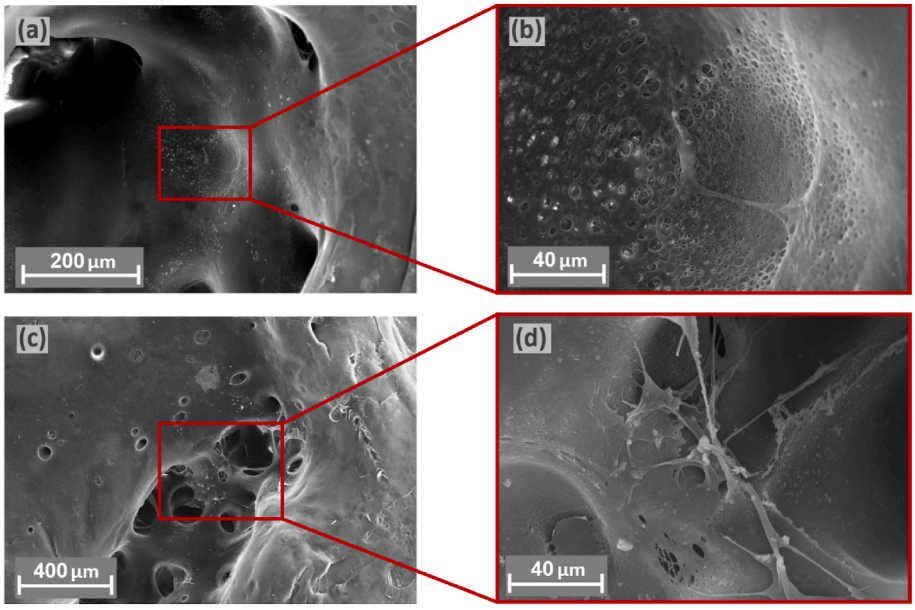

Fig. 6. Representative SEM micrographs showing fibroblasts located inside the pores of surface-modified scaffold samples HA-RP (a) with respective image under higher magnification (b), and on scaffold samples HA-SP (c) with corresponding image under higher magnification (d).

higher levels of actin and collagen I fibres necessary for tissue healing (Ravikanth et al., 2011; Popova et al., 2010; Gunaydin, 2021). A more active phenotype, could prove to be of great value in terms of the development of new connective tissue, essential for the adequate recovery and proper function of a printed PEEK prosthesis, in terms of connective tissue adhesion (Xia et al., 2022; Ravikanth et al., 2011). However, no true conclusions can be taken from the evaluation of the SEM images given that the cells can show vastly different morphologies and thus no direct correlations can be made.

4. Conclusions

Given the potential of 3D-printed PEEK for customized medical devices, previous research has reported on the use of scaffold structures and surface modifications to address PEEK's bioinert nature. Nevertheless, research mainly focuses on bone-related responses using osteoblasts, disregarding the important role of primary connective tissue cells like fibroblasts in the healing process after surgical intervention and the response of these cells to different surface modifications developed to improve 3D-printed PEEK osseointegration. In this work, solid and porous scaffold PEEK samples were 3D-printed and modified to include multi-scale surface features which were tested with fibroblast

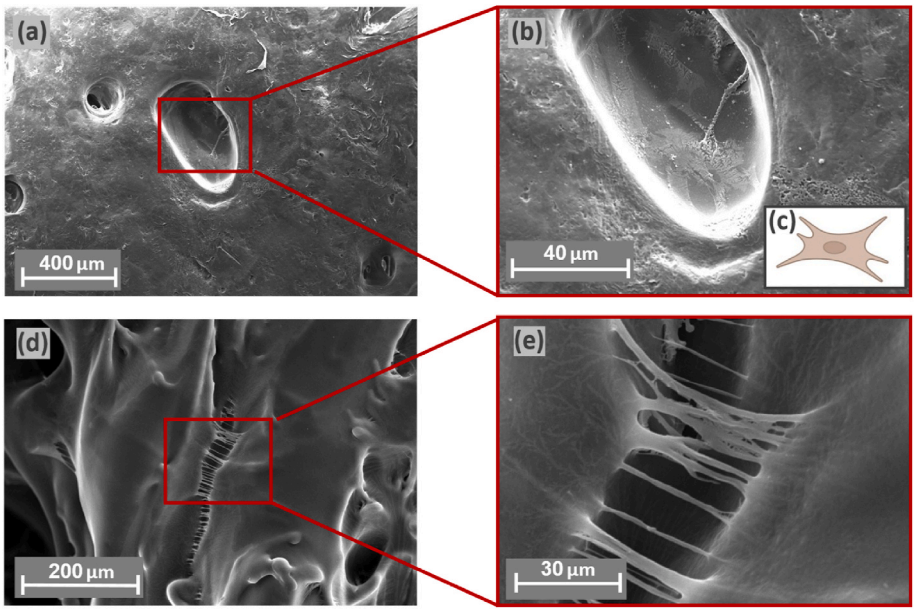

Fig. 7. Representative SEM observations of cells adhered to solid sample HA-R (a) with corresponding image under higher magnification (b) and illustration of cell conformation (c) along with observation of cells adhered to scaffold sample HA-RP (d) with corresponding image under higher magnification of a cluster of cells (e).

cells to study the effects of different 3D-printed PEEK biofunctionalization techniques in connective tissue's response.

The printed PEEK samples varied in design, with solid and porous scaffold samples, and in surface roughness, with both designs printed with smooth and rough surfaces. The porous scaffold design was obtained by tuning the gyroid TPMS dimensions to structural integrity, pore size and interconnectivity requirements which were assessed through micro-CT analysis and compression testing. With this, average pore size of around 450 µm was achieved with scaffold samples with just about 25 % of volume porosity, which is much lower than the porosity of most scaffolds presented in previous literature. In this regard, future investigations can test this proposed design methodology with other TPMS topologies and compare the results on mechanical strength and cell response.

Additionally printed samples were also sulfonated to create a nanoporous network which was then incorporated with hydroxyapatite particles. This resulted in an array of sample configurations with multiscale surface features characterized by surface roughness and wettability measurements and additionally observed using SEM. Fibroblast cell culture assays were conducted on differently functionalized 3D-printed PEEK samples to assess both the individual and combined effects of the tested features in cellular response. Data from these assays suggests that the solid design printed with a rough surface and submitted to both the sulfonation, and HA incorporation procedure presented with samples HA-R constitutes the best environment for connective tissue response. This is supported by the relatively balanced results obtained from fibroblast cultures on samples in all three of the parameters analysed (fibroblast growth, distribution, and metabolic activity). Therefore, the results suggest that HA-R samples, with their modified rough surfaces, constitute the most suitable environment for promoting fibroblast adhesion and proliferation among the tested configurations.

Conversely, the lowest values for these parameters were obtained with as-printed smooth samples S emphasizing the need for surface functionalization of 3D-printed PEEK. Preliminary results from the metabolic activity assay show that, despite their advantages for osseointegration, large-scale porous scaffolds can present an adverse environment for fibroblasts whereas solid surfaces display a more active form of these cells. With fibroblasts, this cellular activity suggests a more active role in the formation of an extracellular matrix that is essential for the support and cohesion of the connective tissues and thus, plays a significant role in the healing process after implantation.

Despite these findings, this work presents some limitations that need to be considered and addressed in future research. The conducted study focuses on short-term *in vitro* fibroblast responses, meaning that long-term evaluations are necessary to gather more conclusive evidence on the effects of these surface features in extracellular matrix deposition and connective tissue integration. Furthermore, the surface features studied in this work, despite their effects in fibroblast responses, require additional analysis of the adjustment of surface characteristics like pore size, sulfonation time or HA concentration. Considering this, further investigations could address these limitations and test the stability of the tested features after prolonged exposure to physiological conditions or under fatigue loading.

The method presented in this work to create a rough and microporous surface incorporated with HA represented by samples HA-R resulted in the best fibroblast adhesion and proliferation profile. However, this method to create rough 3D printed samples also resulted in lower strength and rigidity observed in the compression tests. This would make it difficult to choose this surface modification for orthopaedic applications where mechanical strength is an important requirement. However, 3D-printing provides unique capability to implement these distinct features at different interfaces, yielding Functionally Graded Biomaterial (FGBm) designs that could improve connective tissue adhesion while assuring mechanical property requirements. These 3D-printed structures may also include multi-scale porous characteristics at the bone interface that could be advantageous for osteogenic activity. In this regard, 3D-printing has the potential to create advanced implant solutions where surface features can be tuned for integration with different types of tissue. Considering this, further work is required to assess these multi-scale features in a co-culture format including combinations of cell types that are often overlooked, such as fibroblasts and chondrocytes as these are both central in the connective, tendinous and ligament tissue attachment process. Additionally, in these formats it would be important to include studies both on protein adsorption and on collagen deposition as these are important to establish compatibility and to assess healing potential. With such studies, surface and porous configurations can be optimized for each specific use case, contributing with significant developments to the biofunctionalization of 3D-printed PEEK, and potentially resulting in more advanced implant solutions.

CRediT authorship contribution statement

Pedro Rendas: Writing – original draft, Validation, Investigation, Formal analysis, Conceptualization. **Joana Amorim:** Writing – original draft, Validation, Methodology, Investigation, Formal analysis. **Pedro Viana Baptista:** Writing – review & editing, Validation, Supervision, Resources, Methodology, Conceptualization. **Catarina Vidal:** Writing – review & editing, Visualization, Supervision, Resources. **Lígia Figueiredo:** Writing – review & editing, Visualization, Validation, Supervision. **Alexandra R. Fernandes:** Writing – review & editing, Validation, Supervision, Resources, Methodology, Conceptualization. **Bruno Soares:** Writing – review & editing, Supervision, Resources, Project administration, Methodology.

Declaration of competing interest

The authors declare that they have no known competing financial interests or personal relationships that could have appeared to influence the work reported in this paper.

Acknowledgment

The authors acknowledge Fundação para a Ciência e a Tecnologia (FCT-MCTES) for its financial support through the PhD scholarship UI/BD/151082/2021, through the projects UIDB/00667/2020 and UIDP/00667/2020 of UNIDEMI, the projects UIDP/04378/2020 and UIDB/04378/2020 of the Research Unit on Applied Molecular Biosciences – UCIBIO, the project LA/P/0140/2020 of the Associate Laboratory Institute for Health and Bioeconomy - i4HB and the project NANOHEAT (2022.04315.PTDC). The authors would also like to thank Professor João Sottomayor (LAQV, Department of Chemistry, NOVA School of Science and Technology) for access to the wettability measuring equipment.

Appendix A. Supplementary data

Supplementary data to this article can be found online at https://doi.org/10.1016/j.jmbbm.2025.106979.

Data availability

Data will be made available on request.

References

Abbasi, N., Hamlet, S., Love, R.M., Nguyen, N.T., 2020. Porous scaffolds for bone regeneration. J. Sci. Adv. Mater. Devices. 5, 1–9. https://doi.org/10.1016/j.jsamd.2020.01.007.

Ajami, S., Coathup, M.J., Khoury, J., Blunn, G.W., 2017. Augmenting the bioactivity of polyetheretherketone using a novel accelerated neutral atom beam technique. J. Biomed. Mater. Res. Part B Appl. Biomater. 105, 1438–1446. https://doi.org/10.1002/jbm.b.33681.

Almasi, D., Izman, S., Assadian, M., Ghanbari, M., Abdul Kadir, M.R., 2014. Crystalline ha coating on peek via chemical deposition. Appl. Surf. Sci. 314, 1034–1040. https://doi.org/10.1016/j.apsusc.2014.06.074.

Apium PEEK 450 Natural Datasheet, n.d. https://apiumtec.com/download/apium-peek-450-datasheet.

Bobbert, F.S.L., Lietaert, K., Eftekhari, A.A., Pouran, B., Ahmadi, S.M., Weinans, H., Zadpoor, A.A., 2017. Additively manufactured metallic porous biomaterials based on minimal surfaces: a unique combination of topological, mechanical, and mass transport properties. Acta Biomater. 53, 572–584. https://doi.org/10.1016/j.actbio.2017.02.024.

Briem, D., Strametz, S., Schröoder, K., Meenen, N.M., Lehmann, W., Linhart, W., Ohl, A., Rueger, J.M., 2005. Response of primary fibroblasts and osteoblasts to plasma treated polyetheretherketone (PEEK) surfaces. J. Mater. Sci. Mater. Med. 16, 671–677. https://doi.org/10.1007/s10856-005-2539-z.

Choroba, K., Machura, B., Kula, S., Raposo, L.R., Fernandes, A.R., Kruszynski, R., Erfurt, K., Shul'Pina, L.S., Kozlov, Y.N., Shul'Pin, G.B., 2019. Copper(ii) complexes with 2,2′:6′,2″-terpyridine, 2,6-di(thiazol-2-yl)pyridine and 2,6-di(pyrazin-2-yl)pyridine substituted with quinolines. Synthesis, structure, antiproliferative activity, and catalytic activity in the oxidation of alkanes and alcohols. Dalt. Trans. 48, 12656–12673. https://doi.org/10.1039/c9dt01922g.

Dondani, J.R., Iyer, J., Tran, S.D., 2023. Surface treatments of PEEK for osseointegration to bone. Biomolecules 13. https://doi.org/10.3390/biom13030464.

Elhattab, K., Sikder, P., Walker, J.M., Bottino, M.C., Bhaduri, S.B., 2020. Fabrication and evaluation of 3-D printed PEEK scaffolds containing Macropores by design. Mater. Lett. 263, 127227. https://doi.org/10.1016/j.matlet.2019.127227.

Gao, C., Wang, Y., Han, F., Yuan, Z., Li, Q., Shi, C., Cao, W., Zhou, P., Xing, X., Li, B., 2017. Antibacterial activity and osseointegration of silver-coated poly(ether ether ketone) prepared using the polydopamine-assisted deposition technique. J. Mater. Chem. B 5, 9326–9336. https://doi.org/10.1039/c7tb02436c.

Gibson, I., Rosen, D., Stucker, B., Khorasani, M., 2021. Additive Manufacturing Technologies, Third. Springer International Publishing. https://doi.org/10.1007/978-3-030-56127-7.

Green, S., Schlegel, J., 2001. A polyaryletherketone biomaterial for use in medical implant applications. Polym. Med. Ind. Proc. a Conf. Held Brussels 1–7.

Gugliotta, Y., Zavattero, E., Ramieri, G., Borbon, C., Gerbino, G., 2024. Cranio-maxillofacial reconstruction with polyetheretherketone patient-specific implants: aesthetic and functional outcomes. J. Personalized Med. 14. https://doi.org/10.3390/jpm14080849.

Gunaydin, G., 2021. CAFs interacting with TAMs in tumor microenvironment to enhance tumorigenesis and immune evasion. Front. Oncol. 11, 1–29. https://doi.org/10.3389/fonc.2021.668349.

Huang, R.Y.M., Shao, P., Burns, C.M., Feng, X., 2001. Sulfonation of poly(ether ether ketone)(PEEK): kinetic study and characterization. J. Appl. Polym. Sci. 82, 2651–2660. https://doi.org/10.1002/app.2118.

Huo, S., Meng, X., Zhang, S., Yue, B., Zhao, Y., Long, T., Nie, B., Wang, Y., 2021. Hydrofluoric acid and nitric acid cotreatment for biofunctionalization of polyetheretherketone in M2 macrophage polarization and osteogenesis. J. Biomed. Mater. Res., Part A 109, 879–892. https://doi.org/10.1002/jbm.a.37079.

Jang, T.S., Park, S.J., Lee, J.E., Yang, J., Park, S.H., Jun, M.B.G., Kim, Y.W., Aranas, C., Choi, J.P., Zou, Y., Advincula, R.C., Zheng, Y., Jang, H.L., Cho, N.J., Do Jung, H., Kim, S.H., 2022. Topography-supported nanoarchitectonics of hybrid scaffold for systematically modulated bone regeneration and remodeling. Adv. Funct. Mater. 32. https://doi.org/10.1002/adfm.202206863.

Jarman-Smith, M., Brady, M., Kurtz, S.M., Cordaro, N.M., Walsh, W.R., 2012. Porosity in polyaryletheretherketone. In: PEEK Biomater. Handb., pp. 181–199.

Johansson, P., Barkarmo, S., Hawthan, M., Peruzzi, N., Kjellin, P., Wennerberg, A., 2018. Biomechanical, histological, and computed X-ray tomographic analyses of hydroxyapatite coated PEEK implants in an extended healing model in rabbit. J. Biomed. Mater. Res., Part A 106, 1440–1447. https://doi.org/10.1002/jbm.a.36345.

Karageorgiou, V., Kaplan, D., 2005. Porosity of 3D biomaterial scaffolds and osteogenesis. Biomaterials 26, 5474–5491. https://doi.org/10.1016/j.biomaterials.2005.02.002.

Kumar, R., Kumar, M., Chohan, J.S., 2021. The role of additive manufacturing for biomedical applications: a critical review. J. Manuf. Process. 64, 828–850. https://doi.org/10.1016/j.jmapro.2021.02.022.

Kurtz, S.M., 2012. PEEK Biomaterials Handbook, first ed. Elsevier.

Kurtz, S.M., Devine, J.N., 2007. PEEK biomaterials in trauma, orthopedic, and spinal implants. Biomaterials 28, 4845–4869. https://doi.org/10.1016/j.biomaterials.2007.07.013.

Lee, J.H., Jang, H.L., Lee, K.M., Baek, H.R., Jin, K., Noh, J.H., 2017. Cold-spray coating of hydroxyapatite on a three-dimensional polyetheretherketone implant and its biocompatibility evaluated by in vitro and in vivo minipig model. J. Biomed. Mater. Res. Part B Appl. Biomater. 105, 647–657. https://doi.org/10.1002/jbm.b.33589.

Lenis-Rojas, O.A., Roma-Rodrigues, C., Fernandes, A.R., Marques, F., Pérez-Fernández, D., Guerra-Varela, J., Sánchez, L., Vázquez-García, D., López-Torres, M., Fernández, A., Fernández, J.J., 2017. Dinuclear RuII(bipy)2 derivatives: structural, biological, and in vivo zebrafish toxicity evaluation. Inorg. Chem. 56, 7127–7144. https://doi.org/10.1021/acs.inorgchem.7b00790.

Lewandrowski, K.U., Gresser, J.D., Bondre, S.P., Silva, A.E., Wise, D.L., Trantolo, D.J., 2000. Developing porosity of poly(propylene glycol-co-fumaric acid) bone graft substitutes and the effect on osteointegration: a preliminary histology study in rats. J. Biomater. Sci. Polym. Ed. 11, 879–889. https://doi.org/10.1163/156856200744075.

Li, Y., Wang, J., He, D., Zhu, Guoxiong, Wu, G., Chen, L., 2020. Surface sulfonation and nitrification enhance the biological activity and osteogenesis of polyetheretherketone by forming an irregular nano-porous monolayer. J. Mater. Sci. Mater. Med. 31, 1–12. https://doi.org/10.1007/s10856-019-6349-0.

Ma, R., Tang, T., 2014. Current strategies to improve the bioactivity of PEEK. Int. J. Mol. Sci. 15, 5426–5445. https://doi.org/10.3390/ijms15045426.

Ma, R., Wang, J., Li, C., Ma, K., Wei, J., Yang, P., Guo, D., Wang, K., Wang, W., 2020. Effects of different sulfonation times and post-treatment methods on the characterization and cytocompatibility of sulfonated PEEK. J. Biomater. Appl. 35, 342–352. https://doi.org/10.1177/0885328220935008.

Masamoto, K., Fujibayashi, S., Yabutsuka, T., Hiruta, T., Otsuki, B., Okuzu, Y., Goto, K., Shimizu, T., Shimizu, Y., Ishizaki, C., Fukushima, K., Kawai, T., Hayashi, M., Morizane, K., Kawata, T., Imamura, M., Matsuda, S., 2019. In vivo and in vitro bioactivity of a "precursor of apatite" treatment on polyetheretherketone. Acta Biomater. 91, 48–59. https://doi.org/10.1016/j.actbio.2019.04.041.

Mikos, A.G., Holland, T.A., Fisher, J.P., Jansen, J.A., van der Waerden, J.P.C.M., Vehof, J.W.M., Dean, D., 2002. Soft and hard tissue response to photocrosslinked poly(propylene fumarate) scaffolds in a rabbit model. J. Biomed. Mater. Res. 59, 547–556. https://doi.org/10.1002/jbm.1268.

Misch, C.E., Qu, Z., Bidez, M.W., 1999. Mechanical properties of trabecular bone in the human mandible: implications for dental implant treatment planning and surgical

placement. J. Oral Maxillofac. Surg. 57, 700–706. https://doi.org/10.1016/S0278-2391(99)90437-8.
Morrison, C., Macnair, R., MacDonald, C., Wykman, A., Goldie, I., Grant, M.H., 1995. In vitro biocompatibility testing of polymers for orthopaedic implants using cultured fibroblasts and osteoblasts. Biomaterials 16, 987–992. https://doi.org/10.1016/0142-9612(95)94906-2.
Nsiempba, K.M., Wang, M., Vlasea, M., 2021. Geometrical degrees of freedom for cellular structures generation: a new classification paradigm. Appl. Sci. 11. https://doi.org/10.3390/app11093845.
Ouyang, L., Chen, M., Wang, D., Lu, T., Wang, H., Meng, F., Yang, Y., Ma, J., Yeung, K.W. K., Liu, X., 2019. Nano textured PEEK surface for enhanced osseointegration. ACS Biomater. Sci. Eng. 5, 1279–1289. https://doi.org/10.1021/acsbiomaterials.8b01425.
Panesar, A., Abdi, M., Hickman, D., Ashcroft, I., 2018. Strategies for functionally graded lattice structures derived using topology optimisation for Additive Manufacturing. Addit. Manuf. 19, 81–94. https://doi.org/10.1016/j.addma.2017.11.008.
Popova, E.N., Pletjushkina, O.Y., Dugina, V.B., Domnina, L.V., Ivanova, O.Y., Izyumov, D.S., Skulachev, V.P., Chernyak, B.V., 2010. Scavenging of reactive oxygen species in mitochondria induces myofibroblast differentiation. Antioxidants Redox Signal. 13, 1297–1307. https://doi.org/10.1089/ars.2009.2949.
Porrelli, D., Mardirossian, M., Crapisi, N., Urban, M., Ulian, N.A., Bevilacqua, L., Turco, G., Maglione, M., 2021. Polyetheretherketone and titanium surface treatments to modify roughness and wettability – improvement of bioactivity and antibacterial properties. J. Mater. Sci. Technol. 95, 213–224. https://doi.org/10.1016/j.jmst.2021.04.023.
Ravikanth, M., Soujanya, P., Manjunath, K., Saraswathi, T.R., Ramachandran, C.R., 2011. Heterogenecity of fibroblasts. J. Oral Maxillofac. Pathol. 15, 247–250. https://doi.org/10.4103/0973-029X.84516.
Rendas, P., Figueiredo, L., Machado, C., Mourão, A., Vidal, C., Soares, B., 2022. Mechanical performance and bioactivation of 3D-printed PEEK for high-performance implant manufacture: a review. Prog. Biomater. https://doi.org/10.1007/s40204-022-00214-6.
Rendas, P., Figueiredo, L., Cláudio, R., Vidal, C., Soares, B., 2023. Investigating the effects of printing temperatures and deposition on the compressive properties and density of 3D printed polyetheretherketone. Prog. Addit. Manuf. https://doi.org/10.1007/s40964-023-00550-4.
Restrepo, S., Ocampo, S., Ramirez, J.A., Paucar, C., Garcia, C., 2017. Mechanical properties of ceramic structures based on Triply Periodic Minimal Surface (TPMS) processed by 3D printing. J. Phys. Conf. Ser. 935. https://doi.org/10.1088/1742-6596/935/1/012036.
Rivard, C.H., Rhalmi, S., Coillard, C., 2002. In vivo biocompatibility testing of PEEK polymer for a spinal implant system: a study in rabbits. J. Biomed. Mater. Res. 15, 488–498. https://doi.org/10.1002/jbm.10159.
Sachs, E., Cima, M., Cornie, J., Brancazio, D., Bredt, J., Curodeau, A., Fan, T., Khanuja, S., Lauder, A., Lee, J., Michaels, S., 1993. Three-dimensional printing: the physics and implications of additive manufacturing. CIRP Ann. - Manuf. Technol. 42, 257–260. https://doi.org/10.1016/S0007-8506(07)62438-X.
Sharifi, R., Almasi, D., Bin Sudin, I., Abdul Kadir, M.R., Jamshidy, L., Amiri, S.M., Mozaffari, H.R., Sadeghi, M., Roozbahani, F., Iqbal, N., 2018. Enhancement of the mechanical properties of hydroxyapatite/sulphonated poly ether ether ketone treated layer for orthopaedic and dental implant application. Int. J. Biomater. 2018. https://doi.org/10.1155/2018/9607195.
Spece, H., Yu, T., Law, A.W., Marcolongo, M., Kurtz, S.M., 2020. 3D printed porous PEEK created via fused filament fabrication for osteoconductive orthopaedic surfaces. J. Mech. Behav. Biomed. Mater. 109. https://doi.org/10.1016/j.jmbbm.2020.103850.
Spece, H., DeSantis, P.M., Kurtz, S.M., 2022. Development of an architecture-property model for triply periodic minimal surface structures and validation using material extrusion additive manufacturing with polyetheretherketone (PEEK). J. Mech. Behav. Biomed. Mater. 133. https://doi.org/10.1016/j.jmbbm.2022.105345.
Su, Y., He, J., Jiang, N., Zhang, H., Wang, L., Liu, X., Li, D., Yin, Z., 2020. Additively-manufactured poly-ether-ether-ketone (PEEK) lattice scaffolds with uniform microporous architectures for enhanced cellular response and soft tissue adhesion. Mater. Des. 191, 108671. https://doi.org/10.1016/j.matdes.2020.108671.
Su, Q., Qiao, Y., Xiao, Y., Yang, S., Wu, H., Li, J., He, X., Hu, X., Yang, H., Yong, X., 2023. Research progress of 3D printed poly (ether ether ketone) in the reconstruction of craniomaxillofacial bone defects. Front. Bioeng. Biotechnol. 11, 1–18. https://doi.org/10.3389/fbioe.2023.1259696.
Sunarso, A. Tsuchiya, Fukuda, N., Toita, R., Tsuru, K., Ishikawa, K., 2018. Effect of micro-roughening of poly(ether ether ketone) on bone marrow derived stem cell and macrophage responses, and osseointegration. J. Biomater. Sci. Polym. Ed. 29, 1375–1388. https://doi.org/10.1080/09205063.2018.1461448.
Takaoka, Y., Fujibayashi, S., Onoe, H., Goto, K., Otsuki, B., Kawai, T., Okuzu, Y., Shimizu, T., Ikeda, N., Orita, K., Honda, S., Ikezaki, T., Yabutsuka, T., Matsuda, S., 2024. Bone ingrowth into a porous structure is achieved by preceding fibrogenesis and vascularization. Acta Biomater. 177, 243–252. https://doi.org/10.1016/j.actbio.2024.02.016.
Thieringer, F.M., Honigmann, P., Sharma, N., 2022. Medical Additive Manufacturing in Surgery: Translating Innovation to the Point of Care, pp. 359–376. https://doi.org/10.1007/978-3-030-99838-7_20.
Valainis, D., Dondl, P., Foehr, P., Burgkart, R., Kalkhof, S., Duda, G.N., Van Griensven, M., Poh, P.S.P., 2019. Integrated additive design and manufacturing approach for the bioengineering of bone scaffolds for favorable mechanical and biological properties. Biomed. Mater. 14. https://doi.org/10.1088/1748-605X/ab38c6.
Wang, W., Luo, C.J., Huang, J., Edirisinghe, M., 2019. PEEK surface modification by fast ambient-temperature sulfonation for bone implant applications. J. R. Soc. Interface 16. https://doi.org/10.1098/rsif.2018.0955.
Wang, L., Yang, C., Sun, C., Yan, X., He, J., Shi, C., Liu, C., Li, D., Jiang, T., Huang, L., 2022. Fused deposition modeling PEEK implants for personalized surgical application: from clinical need to biofabrication. Int. J. Bioprinting. 8, 225–243. https://doi.org/10.18063/ijb.v8i4.615.
Weinans, H., Huiskes, R., Grootenboer, H.J., 1992. Effects of material properties of femoral hip components on bone remodeling. J. Orthop. Res. 10, 845–853. https://doi.org/10.1002/jor.1100100614.
Wenz, L.M., Merritt, K., Brown, S.A., Moet, A., Steffee, A.D., 1990. In vitro biocompatibility of polyetheretherketone and polysulfone composites. J. Biomed. Mater. Res. 24, 207–215. https://doi.org/10.1002/jbm.820240207.
Wong, K.I., Zhong, Y., Li, D., Cheng, Z., Yu, Z., Wei, M., 2021. Modified porous microstructure for improving bone compatibility of poly-ether-ether-ketone. J. Mech. Behav. Biomed. Mater. 120, 104541. https://doi.org/10.1016/j.jmbbm.2021.104541.
Xia, D., Wang, Y., Wu, R., Zheng, Q., Zhang, G., Xu, S., Zhou, P., 2022. The effect of pore size on cell behavior in mesoporous bioglass scaffolds for bone regeneration. Appl. Mater. Today 29, 101607. https://doi.org/10.1016/j.apmt.2022.101607.
Yabutsuka, T., Fukushima, K., Hiruta, T., Takai, S., Yao, T., 2017. Effect of pores formation process and oxygen plasma treatment to hydroxyapatite formation on bioactive PEEK prepared by incorporation of precursor of apatite. Mater. Sci. Eng. C. 81, 349–358. https://doi.org/10.1016/j.msec.2017.07.017.
Yabutsuka, T., Fukushima, K., Hiruta, T., Takai, S., Yao, T., 2018. Fabrication of bioactive fiber-reinforced PEEK and MXD6 by incorporation of precursor of apatite. J. Biomed. Mater. Res. Part B Appl. Biomater. 106, 2254–2265. https://doi.org/10.1002/jbm.b.34025.
Zhang, W., Liu, L., Zhou, H., He, C., Yang, X., Fu, J., Wang, H., Liu, Y., Zheng, Y., 2023. Surface bisphosphonation of polyetheretherketone to manipulate immune response for advanced osseointegration. Mater. Des. 232, 112151. https://doi.org/10.1016/j.matdes.2023.112151.
Zhang, Y., Zhang, W., Yang, M., Mengqi, L., Zhou, L., Liu, Y., Liu, L., Zheng, Y., 2025. Comprehensive review of polyetheretherketone use in dentistry. J. Prosthodont. Res. https://doi.org/10.2186/jpr.JPR_D_24_00142.
Zhao, Y., Wong, H.M., Wang, W., Li, P., Xu, Z., Chong, E.Y.W., Yan, C.H., Yeung, K.W.K., Chu, P.K., 2013. Cytocompatibility, osseointegration, and bioactivity of three-dimensional porous and nanostructured network on polyetheretherketone. Biomaterials 34, 9264–9277. https://doi.org/10.1016/j.biomaterials.2013.08.071.
Zheng, Y., Xiong, C., Wang, Z., Zhang, L., 2015. Enhanced osteoblast cells adhesion, spreading, and proliferation to surface-carboxylated poly(etheretherketone), J. Bioact. Compat. Polym. 30, 302–318. https://doi.org/10.1177/0883911515572494.